Dispersion-curve imaging nonuniqueness studies from multi-channel analysis of surface waves (MASW) using synthetic seismic data

Julian Ivanov, J. Tyler Schwenk, Richard D. Miller, and Shelby Peterie*
Kansas Geological Survey, The University of Kansas

Summary

We use the multi-channel analysis of surface waves (MASW) method to analyze synthetic seismic data calculated from models that produce very similar high-velocity dispersion curve gradients at low frequencies. The MASW dispersion-curve images of the Rayleigh wave were obtained from data calculated using simple layered models with high (2-layer) and gradual (10-layer) shear-wave velocity (V_s) vertical gradients. The tests demonstrated that, for most of the frequency range, the corresponding dispersion-curve images are near identical with a high-velocity-gradient along low frequencies (HVGLF). The HVGLF trend obtained from the 2-layer model is a result of fundamental-mode Rayleigh-wave transitioning into the first higher mode, a 'mode kissing.' The HVGLF trend obtained from the 10-layer model is a result of only the fundamental-mode Rayleigh wave. It was observed that such nonuniqueness can lead to erroneous interpretation of dispersion events and consequent V_s inversion results. Further analysis showed that dispersion curve image patterns differ at relatively very low and very high frequency ranges. As a result, it was concluded that it might be possible to obtain evidence of how to interpret HVGLF dispersion curve images by observing specific patterns that fall outside the main HVGLF dispersion-curve feature at lower and higher frequencies.

Introduction

Stiffness properties of near-surface materials are important for various environmental and engineering applications. Stiffness is directly related to shear-wave velocity (V_s), which increases as material shear strength (stiffness, rigidity) increases. V_s can be estimated by analyzing surface waves on seismic data records. We use the multichannel analysis of surface waves (MASW) method to estimate near-surface shear-wave velocity from high-frequency (≥ 2 Hz) Rayleigh-wave data (Miller et al., 1999a; Song et al., 1989; Park et al., 1999; Xia et al., 1999a). Shear-wave velocities estimated using MASW have reliably and consistently correlated with drill data. Using the MASW method, Xia et al. (2000) non-invasively measured V_s within 15% of V_s measured in wells. Miller et al. (1999a) mapped bedrock with 0.3-m (1-ft) accuracy at depths of about 4.5-9 m (15-30 ft), as confirmed by numerous borings.

The MASW method has been applied to problems such as characterization of pavements (Ryden et al., 2004), the study of Poisson's ratio (Ivanov et al., 2000), study of levees and subgrade (Ivanov et al., 2005; Ivanov et al., 2006b), investigation of sea-bottom sediment stiffness (Ivanov et al., 2000; Kaufman et al., 2005; Park et al., 2005a), mapping of fault zones (Ivanov et al., 2006c), study of Arctic ice sheets (Ivanov et al., 2009, Tsoflias et al., 2008), detection of dissolution features (Miller et al., 1999b), and measurement of S-wave velocity as a function of depth (Xia et al., 1999b). Studies of the MASW method have been extended to areas of determination of near-surface Q (Xia et al., 2002) and the acquisition of more realistic compressional-wave refraction models (Ivanov et al., 2006a; Ivanov et al., 2010). A detailed review of established approaches of surface wave methods (SWM) can be found in Socco et al. (2010).

The MASW method is applied by performing the following steps. A single seismic-data record is acquired using a set of low-frequency (e.g., 4.5 Hz) geophones evenly spaced along a line. The seismic data from such a shot record are transformed into a dispersion-curve image (i.e., phase-velocity – frequency domain image), which is used to evaluate the dispersion-curve trend of the fundamental-mode (most often) of the Rayleigh wave. The estimated dispersion curve is then inverted to produce a 1D V_s model (Xia et al., 1999a), which is assigned to the middle of the geophone spread. By assembling numerous 1D V_s models, derived from consecutive seismic shot records acquired along a seismic line, a 2D V_s model can be obtained.

Most recent developments of the MASW method include the expansion of the traditional fundamental-mode dispersion-curve inversion with the inclusion and inversion of higher modes (Xia et al., 2003; Beaty et al., 2002; Beaty and Schmitt, 2003; Luo et al., 2007). It was reported that the addition of first and second higher-mode dispersion curves reduced the relative error of inversion results (compared to borehole data) to 3.6% in comparison to 15% when the fundamental-mode was used only.

However, some researchers have reported that, at some sites, higher-mode energy can dominate the fundamental mode at the low-frequency end of the spectrum (Park et al., 2005b, Ivanov et al., 2009) in a manner that suppresses the fundamental-mode energy at those low frequencies, merges in appearance with fundamental mode trend and can thus lead to mode misinterpretation and overestimation (because of the higher phase velocities of the higher mode). Such higher-mode domination was demonstrated using models with high

DOI http://dx.doi.org/10.1190/segam2013-0425.1

shear-wave velocity contrasts (O'Neill and Matsuoka, 2005; Levshin and Panza, 2006; Calderon and Luke, 2010; Cercato et al., 2010). One of the models suggested by Levshin and Panza (2006) consisted of two layers (Table 1) and had high contrast for both shear (V_s) and compressional (V_p) wave velocities.

Table 1. The two-layer model parameters used for the calculation of synthetic seismic data.

Layer	V_s(m/s)	V_p(m/s)	Dens. (g/m^3)	Thick (m)
1	500	1000	1.8	10
2	1500	3000	1.8	∞

The 2-layer model parameters were used by two different modeling algorithms. One (Zeng et al., 2011) was used to calculate a synthetic seismic record (Figure 1).

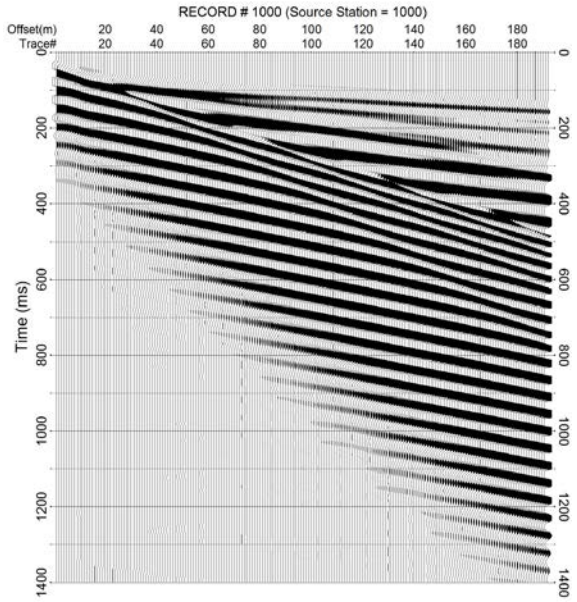

Figure 1. Synthetic seismic data estimated using the velocity model in Table 1.

Another algorithm (Schwab and Knopoff, 1972) was used to calculate the theoretical dispersion curves of the fundamental and the first higher modes. The synthetic seismic record was used to generate a corresponding dispersion-curve image (Park et al., 1998), on which the theoretical dispersion curves were plotted for comparison (Figure 2).

These results (Figure 2) were similar to Cercato et al. (2010). They illustrate that when dealing with such high-velocity-contrast models the dispersion-curve image is dominated by higher-mode energy below a certain frequency (i.e., 20 Hz on Figure 2) instead of the expected fundamental-mode. Consequently, the V_s and corresponding rigidity can be significantly overestimated (e.g., after inversion), potentially leading to detrimental consequences.

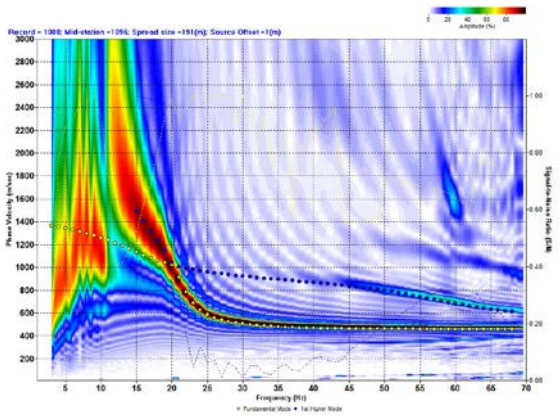

Figure 2. Dispersion-curve image of the synthetic seismic record from the 2-layer model and the estimated fundamental (yellow dots) and first higher (dark dots) modes.

If the dominant dispersion-curve energy trend between 15-70 Hz is properly identified as consisting of two modes (as fundamental mode between 20-70 Hz and as higher mode between 15-20 Hz ranges), a 10-layer inversion will produce a model with Vs values very close to those of the true 2-layer model (Figure 3).

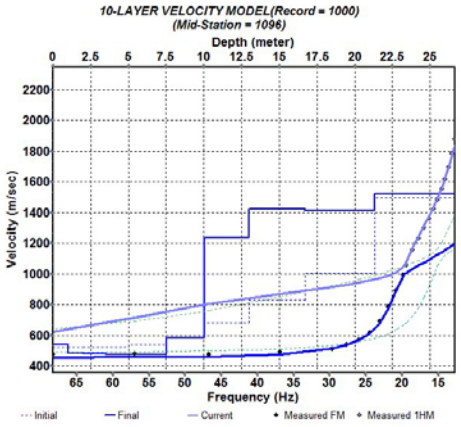

Figure 3. 1D V_s inversion result from interpreting the 2-layer model dispersion-curve trend as fundamental mode in 20-70 Hz and higher mode in 15-20 Hz ranges.

However, such mode recognition and accurate mode separation is unrealistic because there is no evidence to follow. It is most likely to interpret the dominant trend between 15-70 Hz as the fundamental mode. Inverting the misidentified higher-mode portion (15-20 Hz) as part of the fundamental-mode dispersion curve would result in a 10-layer Vs model (Table 2) with values gradually increasing with depth (Figure 4).

DOI http://dx.doi.org/10.1190/segam2013-0425.1

Table 2 The 10-layer model parameters used for the calculation of synthetic seismic data.

Layer	V_s(m/s)	V_p(m/s)	Dens. (g/m^3)	Thick (m)
1	870	2130	1.55	1.9
2	393	961	1.60	2.3
3	384	941	1.65	2.9
4	859	2105	1.70	3.6
5	1099	2692	1.75	4.6
6	1180	2891	1.80	5.7
7	1258	3082	1.85	6.9
8	1452	3558	1.90	8.9
9	1775	4349	1.95	10.9
10	3000	7363	2.00	10.9

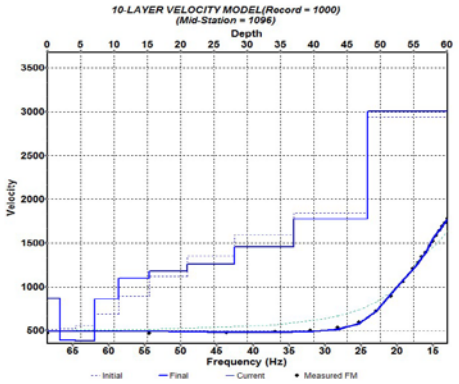

Figure 4. 1D V_s inversion result from interpreting the 2-layer model dispersion-curve trend as fundamental mode between 15-70 Hz range and thus misinterpreting higher-mode between 15-20 Hz.

We then generated a synthetic seismogram for the 10-layer model and compared the calculated dispersion-curve image with that of Figure 2. The main goal was to identify specific features in the dispersion-curve images that would help discern one from another, match the corresponding velocity model, and aid mode interpretation, if possible. However, examination of the dispersion-curve images indicated that they are almost indistinguishable, except in the frequency range below 13 Hz.

Results

The synthetic seismic data for the 2-layer model (Table 1) was calculated for a record with 192 channels with receivers spaced every 1 m, the source was 1 m away from the first geophone, and the source signature was a 20 Hz Ricker wavelet (Figure 1). Then the same parameters were used to calculate the synthetic seismic data (Figure 5) for the 10-layer model (Table 2), from which a dispersion-curve image was obtained (Figure 6). The synthetic seismograms of both models look almost identical.

Dispersion-curve images from the two different models (Figure 2 and Figure 6) appear similar across most frequencies. The energy blob between 7-12 Hz and at about 1200-1300 m/s on Figure 2 is the main difference. This energy band stands apart from the high-velocity gradient between 13-25 Hz. Such a feature is not present on the dispersion-curve image from the 10-layer model, at which the energy between 13-25 Hz becomes smeared at velocities above 2200 m/s.

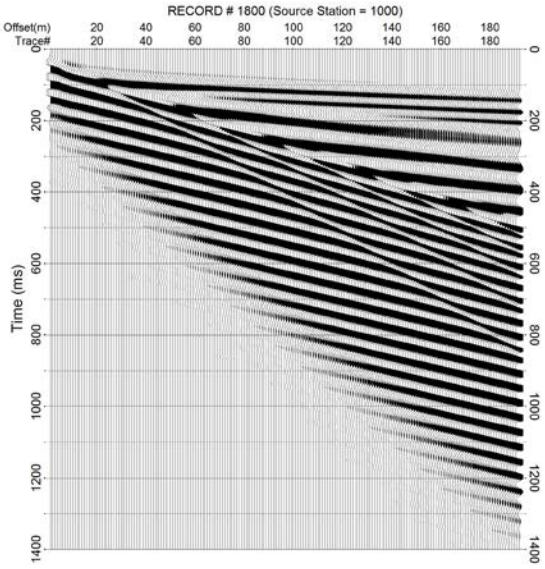

Figure 5. Synthetic seismic data calculated using the velocity model in Table 1.

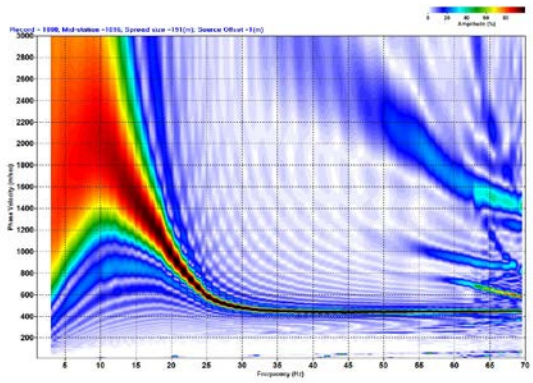

Figure 6. Dispersion-curve image of the 10-layer synthetic seismic record.

Thus, observing such an energy blob on images from real data can potentially help us interpret that we are dealing with a high-contrast velocity model and that the dispersion-curve image trend at low frequencies could be a merger between the fundamental and first higher modes.

DOI http://dx.doi.org/10.1190/segam2013-0425.1

However, it is more difficult to find differences when imaging frequencies above 13 Hz (Figures 7 and 8). Still, the dispersion curve image from the high-velocity contrast 2-layer model has strong higher-mode energy between 45-60 Hz at about 700-850 m/s (Figure 2), an observation not consistent with the 10-layer model dispersion-curve image (Figure 6). Few differences between the dispersion-curve images can be noticed between 60-70 Hz from other higher-mode events. Furthermore, the dispersion-curve images from the two models are practically identical between 13-45 Hz (Figures 9-10). There are no features that could provide any clues as to which image was derived from which model. In such cases, unique image interpretation is not possible.

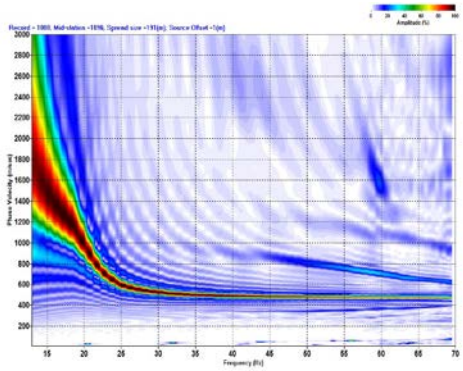

Figure 7. Dispersion-curve image of the synthetic seismic record from the 2-layer model above 13 Hz.

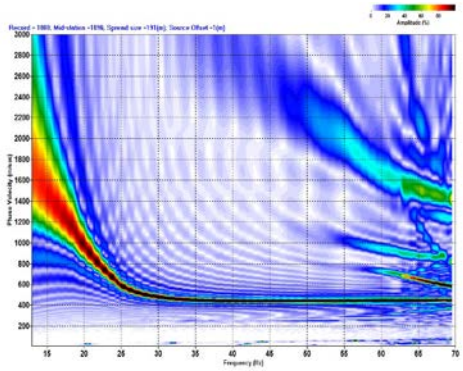

Figure 8. Dispersion-curve image of the synthetic seismic record from the 10-layer model above 13 Hz.

Conclusions

This work demonstrated that two different velocity models, one 2-layer high-velocity contrast model and another 10-layer gradual-velocity model, can have near identical dispersion-curve images within a specific frequency range, i.e., if the data in not sufficiently broad band. Thus, it can be inferred that unique interpretation of such images is not possible and that there are two or more dispersion-curve-pattern interpretations and subsequent inversion results. This we consider to be the main contribution of our research.

When having images with sufficiently wide frequency range (3-70 Hz) there are features that could potentially help separate these two images (such as the energy blob at low frequencies and velocities). Still, these features do not clearly stand out, could easily be attributed to noise or heterogeneities in real data, or may not be available due to poor source or site characteristics. If recognizable, however, they could prevent the misinterpretation of the fundamental mode and resulting V_s overestimation at depth and encourage other approaches for accurate mode estimations.

Presented similarities between the two synthetic data sets suggest the possibilities for difficulties, instabilities, or nonuniqueness with other inversion algorithms, such as full-waveform-inversion.

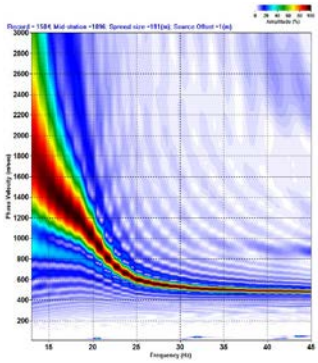

Figure 9. Dispersion-curve image of the synthetic seismic record from the 2-layer model between 13-45 Hz.

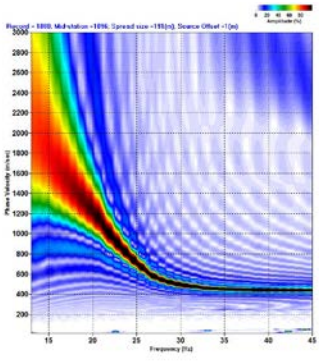

Figure 10. Dispersion-curve image of the synthetic seismic record from the 10-layer model between 13-45 Hz.

Acknowledgments

We appreciate Mary Brohammer's assistance in manuscript preparation.

DOI http://dx.doi.org/10.1190/segam2013-0425.1

http://dx.doi.org/10.1190/segam2013-0425.1

EDITED REFERENCES

Note: This reference list is a copy-edited version of the reference list submitted by the author. Reference lists for the 2013 SEG Technical Program Expanded Abstracts have been copy edited so that references provided with the online metadata for each paper will achieve a high degree of linking to cited sources that appear on the Web.

REFERENCES

Beaty, K. S., and D. R. Schmitt, 2003, Repeatability of multimode Rayleigh-wave dispersion studies: Geophysics, **68**, 782–790, http://dx.doi.org/10.1190/1.1581031.

Beaty, K. S., D. R. Schmitt, and M. Sacchi, 2002, Simulated annealing inversion of multimode Rayleigh wave dispersion curves for geological structure: Geophysical Journal International, **151**, 622–631, http://dx.doi.org/10.1046/j.1365-246X.2002.01809.x.

Calderón-Macías, C., and B. Luke, 2010, Sensitivity studies of fundamental- and higher-mode Rayleigh-wave phase velocities in some specific near-surface scenarios, *in* R. D. Miller, J. D. Bradford, and K. Holliger, eds., Advances in near-surface seismology and ground-penetrating radar: SEG, 185–199.

Cercato, M., F. Cara, E. Cardarelli, G. Di Filippo, G. Di Guilio, and G. Milana, 2010, Surface wave velocity profiling at sites with high stiffness contrast: A comparison between invasive and noninvasive methods: Near Surface Geophysics, **8**, 75–94.

Ivanov, J., R. D. Miller, J. B. Dunbar, and S. Smullen, 2005, Time-lapse seismic study of levees in southern Texas: 75th Annual International Meeting, SEG, Expanded Abstracts, 1121–1124.

Ivanov, J., R. D. Miller, P. J. Lacombe, C. D. Johnson, and J. W. Lane, Jr., 2006a, Delineating a shallow fault zone and dipping bedrock strata using multichannel analysis of surface waves (MASW) seismic method with a land streamer: Geophysics, **71**, no. 5, A39–A42, http://dx.doi.org/10.1190/1.2227521.

Ivanov, J., R. D. Miller, N. Stimac, R. F. Ballard, J. B. Dunbar, and S. Smullen, 2006b, Time-lapse seismic study of levees in southern Texas: 76th Annual International Meeting, SEG, Expanded Abstracts, 3255–3258.

Ivanov, J., R. D. Miller, and G. Tsoflias, 2009, Practical aspects of MASW inversion using varying density: 22nd Symposium on the Application of Geophysics to Engineering and Environmental Problems (SAGEEP), EEGS, Extended Abstracts, 171–177.

Ivanov, J., R. D. Miller, J. Xia, J. B. Dunbar, and S. L. Peterie, 2010, Refraction nonuniqueness studies at levee sites using the refraction-tomography and JARS methods, *in* R. D. Miller, J. D. Bradford, and K. Holliger, eds., Advances in near-surface seismology and ground-penetrating radar: SEG, 327–338.

Ivanov, J., R. D. Miller, J. Xia, D. Steeples, and C. B. Park, 2006a, Joint analysis of refractions with surface waves — An inverse solution to the refraction-traveltime problem: Geophysics, **71**, no. 6, R131–R138, http://dx.doi.org/10.1190/1.2360226.

Ivanov, J. M., C. B. Park, R. D. Miller, and J. Xia, 2000, Mapping Poisson's ratio of unconsolidated materials from a joint analysis of surface-wave and refraction events: 13th Symposium on the Application of Geophysics to Engineering and Environmental Problems (SAGEEP), EEGS, Extended Abstracts, 11–19.

Ivanov, J., S. Peterie, C. D. Johnson, J. W. Lane, R. D. Miller, and D. Clemens, 2009, Near-surface evaluation of Ball Mountain dam, Vermont, using multi-channel analysis of surface waves (MASW)

and refraction tomography seismic methods on land-streamer data: 79th Annual International Meeting, SEG, Expanded Abstracts, 1454–1458.

Kaufmann, R. D., J. Xia, R. Benson, L. B. Yuhr, D. W. Casto, and C. B. Park, 2005, Evaluation of MASW data acquired with a hydrophone streamer in a shallow marine environment: Journal of Environmental & Engineering Geophysics, **10**, no. 2, 87–98, http://dx.doi.org/10.2113/JEEG10.2.87.

Levshin, A. L., and G. F. Panza, 2006, Caveats in multi-modal inversion of seismic surface wavefields: Pure and Applied Geophysics, **163**, 1215–1233, http://dx.doi.org/10.1007/s00024-006-0069-3.

Luo, Y., J. Xia, J. Liu, Q. Liu, and S. Xu, 2007, Joint inversion of high-frequency surface waves with fundamental and higher modes: Journal of Applied Geophysics, **62**, no. 4, 375–384, http://dx.doi.org/10.1016/j.jappgeo.2007.02.004.

Miller, R. D., J. Xia, C. B. Park, J. Davis, W. Shefchik, and L. Moore, 1999b, Seismic techniques to delineate dissolution features in the upper 1000 ft at a power plant site: 69th Annual International Meeting, SEG, Expanded Abstracts, 492–495.

Miller, R. D., J. Xia, C. B. Park, and J. M. Ivanov, 1999a, Multichannel analysis of surface waves to map bedrock: The Leading Edge, **18**, 1392–1396, http://dx.doi.org/10.1190/1.1438226.

O'Neill, A., and T. Matsuoka, 2005, Dominant higher surface-wave modes and possible inversion pitfalls: Journal of Environmental & Engineering Geophysics, **10**, 185–201, http://dx.doi.org/10.2113/JEEG10.2.185.

Park, C. B., R. D. Miller, N. Ryden, J. Xia, and J. Ivanov, 2005b, Combined use of active and passive surface waves: Journal of Environmental & Engineering Geophysics, **10**, 323–334, http://dx.doi.org/10.2113/JEEG10.3.323.

Park, C. B., R. D. Miller, and J. Xia, 1998, Imaging dispersion curves of surface waves on multi-channel record: 68th Annual International Meeting, SEG, Expanded Abstracts, 1377–1380.

Park, C. B., R. D. Miller, J. Xia, J. Ivanov, G. V. Sonnichsen, J. A. Hunter, R. L. Good, R. A. Burns, and H. Christian, 2005a, Underwater MASW to evaluate stiffness of water-bottom sediments: The Leading Edge, **24**, 724–728, http://dx.doi.org/10.1190/1.1993267.

Ryden, N., C. B. Park, P. Ulriksen, and R. D. Miller, 2004, Multimodal approach to seismic pavement testing: Journal of Geotechnical and Geoenvironmental Engineering, **130**, 636–645, http://dx.doi.org/10.1061/(ASCE)1090-0241(2004)130:6(636).

Schwab, F. A., and L. Knopoff, 1972, Fast surface wave and free mode computations, *in* B. A. Bolt, ed., Methods in computational physics: Academic Press, 87–180.

Socco, L. V., S. Foti, and D. Boiero, 2010, Surface-wave analysis for building near-surface velocity models — Established approaches and new perspectives: Geophysics, **75**, no. 5, 75A83–75A102.

Song, Y. Y., J. P. Castagna, R. A. Black, and R. W. Knapp, 1989, Sensitivity of near-surface shear-wave velocity determination from Rayleigh and Love waves: 59th Annual International Meeting, SEG, Expanded Abstracts, 509–512.

Tsoflias, G. P., J. Ivanov, S. Anandakrishnan, H. Horgan, L. Peters, D. Voigt, and P. Winberry, 2008, Firn and shallow ice profiling at Jakobshavn glacier using dispersed seismic surface waves: EOS, Transactions American Geophysical Union, **89**, no. 53, C11D-0528.

Xia, J., R. D. Miller, and C. B. Park, 1999a, Estimation of near-surface shear-wave velocity by inversion of Rayleigh waves: Geophysics, **64**, 691–700, http://dx.doi.org/10.1190/1.1444578.

Xia, J., R. D. Miller, C. B. Park, J. A. Hunter, and J. B. Harris, 1999b, Evaluation of the MASW technique in unconsolidated sediments: 69th Annual International Meeting, SEG, Expanded Abstracts, 437–440.

Xia, J., R. D. Miller, C. B. Park, J. A. Hunter, and J. B. Harris, 2000, Comparing shear-wave velocity profiles from MASW with borehole measurements in unconsolidated sediments, Fraser River delta, B.C., Canada: Journal of Environmental & Engineering Geophysics, **5**, no. 3, 1–13, http://dx.doi.org/10.4133/JEEG5.3.1.

Xia, J., R. D. Miller, C. B. Park, and G. Tian, 2002, Determining *Q* of near-surface materials from Rayleigh waves: Journal of Applied Geophysics, **51**, no. 2-4, 121–129, http://dx.doi.org/10.1016/S0926-9851(02)00228-8.

Xia, J., R. D. Miller, C. B. Park, and G. Tian, 2003, Inversion of high frequency surface waves with fundamental and higher modes: Journal of Applied Geophysics, **52**, no. 1, 45–57, http://dx.doi.org/10.1016/S0926-9851(02)00239-2.

Zeng, C., J. H. Xia, R. D. Miller, and G. P. Tsoflias, 2011, Application of the multiaxial perfectly matched layer (M-PML) to near-surface seismic modeling with Rayleigh waves: Geophysics, **76**, no. 3, T43–T52, http://dx.doi.org/10.1190/1.3560019.